International Journal of Biological Macromolecules 334 (2025) 148756

Contents lists available at ScienceDirect

International Journal of Biological Macromolecules

journal homepage: www.elsevier.com/locate/ijbiomac

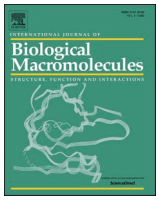

Tough and multifunctional soy protein adhesive via nature-mimetic structural design

Guoyan Zuo [a], Feng Zhu [a], Guodong Zeng [a], Ying Zhou [a], Jiongjiong Li [a], Qiang Gao [b], Jing Luo [a,*], Zeli Que [a,*], Jianzhang Li [b,*]

[a] Co-Innovation Center of Efficient Processing and Utilization of Forest Resources, College of Materials Science and Engineering, Nanjing Forestry University, Nanjing, 210037, China

[b] MOE Key Laboratory of Wooden Material Science and Application, Beijing Forestry University, Qinghua East Road 35, Haidian District, Beijing, 100083, China

ARTICLE INFO

Keywords:
Soy protein adhesive
Nature-mimetic structure
Toughness

ABSTRACT

In response to the growing demands for environmental protection and sustainable growth, the development of multifunctional, formaldehyde-free adhesives has emerged as a significant research direction within the field of materials science. Inspired by the robust structure of spider silk (composed of densely packed rigid crystalline regions and loosely arranged amorphous domains), this study employs epoxidized melamine prepolymer (EM) to react with active groups on soy protein, establishing a rigid cross-linked network. A flexible polyester, ESS, is incorporated into the adhesive system via hydrogen bonding, serving as a buffer layer to mitigate stress impact and dissipate strain energy. Compared with unmodified soy protein adhesive, the incorporation of a biomimetic structure in the adhesive system enhanced the prepressing strength of the SME/10ESS adhesive to 0.78 MPa, reflecting a 333.3 % improvement. Under dry and wet conditions, the shear strength reached 2.01 MPa and 1.12 MPa, showing increases of 42.6 % and 261.3 %, respectively. The work of adhesion increased by 212.5 %, reaching 225 mJ, indicating a significant improvement in toughness. Furthermore, the modified adhesive exhibited broad substrate compatibility and excellent water resistance, suggesting promising applications in wood processing, ceramic restoration, and related fields. The biomimetic modification also significantly enhanced mold resistance, enabling the fresh adhesive to remain mold-free for 12 days under controlled humidity. A life cycle assessment confirms that this biomimetic versatile bio-based adhesive represents a viable alternative to conventional petroleum-based adhesives. Its implementation is of critical significance in addressing the challenges posed by global resource scarcity and climate warming.

1. Introduction

Adhesives are indispensable in wide range of applications, from construction to electronics, where they ensure material cohesion and structural integrity [1,2]. Currently, the most widely used wood adhesives across various sectors are derived from fossil-based polymers, such as formaldehyde-based resins and epoxy adhesives [3–5]. However, these materials are associated with the release of formaldehyde or volatile organic compounds (VOCs) during production and application, posing risks to both environmental and human health [6,7]. In light of increasing petroleum resource depletion and growing environmental concerns, research efforts have shifted toward the development of green, renewable, and easily processable alternatives [8–11]. Soybean meal (SM), an abundant agricultural byproduct, has emerged as a primary candidate for bio-based adhesive research due to its low cost and processability [12–14]. To address the weak intermolecular interactions and poor water resistance of protein-based adhesives, crosslinkers such as polyamide-epichlorohydrin (PAE) are often introduced [15–17]. Nevertheless, as crosslinking density increases, SM adhesives tend to exhibit elevated brittleness and reduced toughness, resulting in cracking and fracture under mechanical stress [18,19]. Consequently, achieving high strength while improving toughness of SM adhesives remains a critical scientific challenge.

Nature has long served as an abundant source of inspiration for advances in numerous scientific fields [20–22]. Spider silk, a quintessential high-toughness material in nature, derives its exceptional toughness from a unique microstructure characterized by the synergistic interplay between crystalline and amorphous regions [23,24]. The crystalline

* Corresponding authors.
E-mail addresses: jingluo@njfu.edu.cn, luojing.rowe@gmail.com (J. Luo), zelique@njfu.edu.cn (Z. Que), lijzh@bjfu.edu.cn (J. Li).

https://doi.org/10.1016/j.ijbiomac.2025.148756
Received 4 August 2025; Received in revised form 30 October 2025; Accepted 3 November 2025
Available online 21 November 2025

regions, primarily composed of polyalanine chains, form β-sheet structures that constitute densely packed domains, exhibiting high strength and rigidity. These regions function as the rigid phase capable of withstanding substantial tensile forces. In contrast, the amorphous regions, rich in glycine sequences, typically adopt α-helical or random coil conformations, creating loosely structured domains. These regions act as the soft phase, enabling energy dissipation and stress relaxation, thereby further enhancing mechanical performance. The cooperative behavior between these structural components endows spider silk with both high strength and remarkable toughness. The microstructure and toughening mechanism of spider silk offer valuable insights for the design of high-strength, high-toughness biomass-based adhesives [25].

Polyesters represent a class of high-performance polymeric materials widely utilized in packaging, construction, and other industries. Through modification or functionalization, they can be employed to synergistically enhance the chemical and physical properties of other polymeric materials [26,27]. However, the conventional production of polyesters relies on non-renewable petroleum resources and is associated with environmental pollution and recycling difficulties. As a green and sustainable alternative, bio-based polyesters hold significant research and application potential [28,29]. With ongoing optimization of raw materials, synthesis techniques, and performance characteristics, bio-based polyesters are expected to emerge as mainstream polymeric materials in the future, contributing substantially to global sustainable development [30,31]. In this study, a bio-based polyester (ESS) was synthesized via esterification polycondensation of epoxidized soybean oil and sebacic acid (Fig. 1b). Both raw materials are derived from renewable resources-soybean oil and castor oil-ensuring environmental sustainability [32–34]. When incorporated into the rigid adhesive crosslinking system, this flexible polymer enhances toughness by facilitating energy dissipation and stress relaxation [35,36]. Thus, the synthesis of bio-based polyester ESS from epoxidized soybean oil and sebacic acid to reinforce soy protein adhesive offers a novel design strategy for toughening bio-based adhesive systems (Fig. 1c).

Innovative development of biomimetic soy protein adhesive with high strength and toughness based on biomimetic principles and inspired by the unique structural characteristics of spider silk, a novel soy protein adhesive with both high strength and toughness was developed in this study. A dense cross-linked network structure was first formed through the reaction between crosslinking agents and soy protein. Subsequently, the flexible bio-based polyester ESS was introduced into the cross-linked soy protein adhesive system via hydrogen bonding interactions, serving as a soft-phase buffer layer to mitigate stress impact and provide energy dissipation. This biomimetic design combining rigid and flexible components not only achieved an optimal balance of mechanical properties but also significantly improved the comprehensive performance of the adhesive. The biomimetically constructed bio-based adhesive demonstrates excellent adhesive application performance and prepressing properties, while simultaneously exhibiting remarkable mold resistance and flame retardancy [37]. These characteristics effectively enhance the stability of bonded products and production efficiency. This study provides a practical solution for developing versatile bio-based adhesives and offers important support for promoting the development of green wood processing industries.

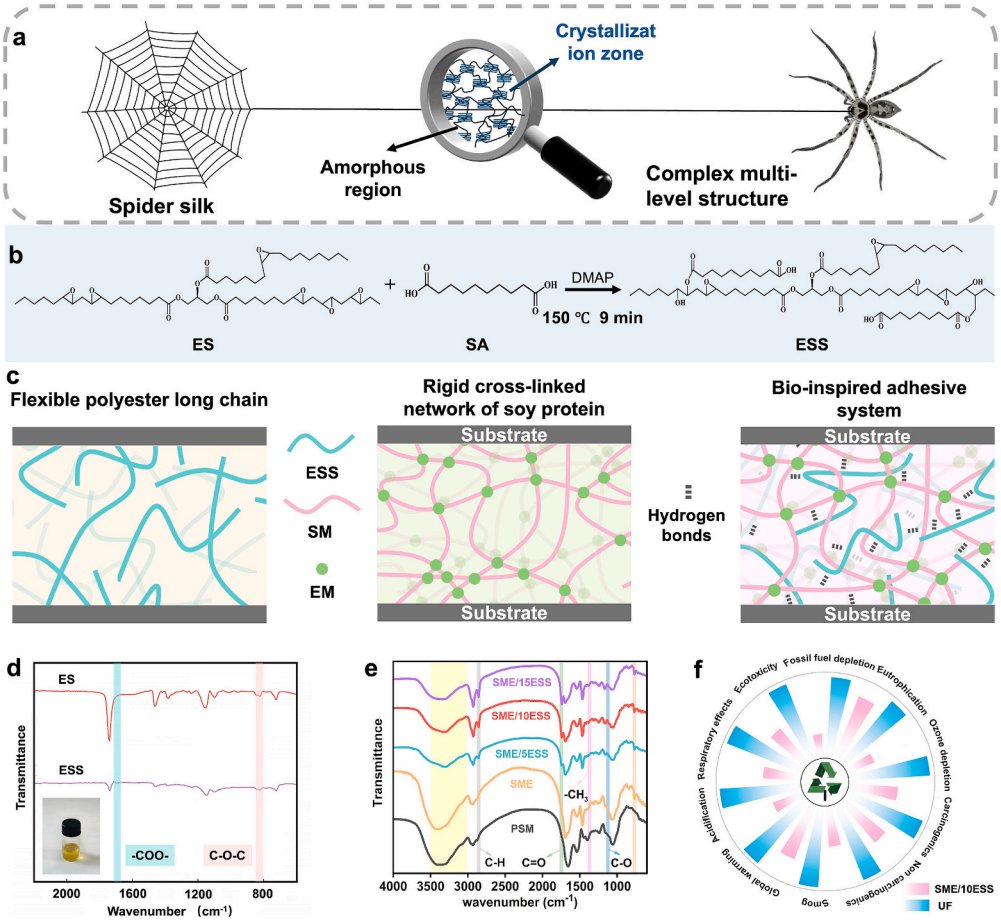

Fig. 1. (a) The unique structural characteristics of spider silk; (b) Molecular formula of bio-based polyester synthesized through esterification reaction between epoxidized soybean oil and sebacic acid; (c) Schematic diagram of ESS-enhanced soy protein adhesive with soft-hard phase structure; (d) Physical image of ESS and its ATR-FT-IR comparison with ES; (e) FT-IR spectra of SM-based adhesive; (f) LCA Comparison between SME/10ESS and UF.

2. Materials and methods

2.1. Materials

Soybean meal (SM), containing 46 wt% protein, 30–34 wt% carbohydrates, and 8.7 wt% moisture, was supplied by Yuwang Ecological Food Industry Co., Ltd. (Shandong, China). The raw materials used in this study were procured from a single production batch and were thoroughly homogenized through physical mixing prior to the commencement of experiments. They were subsequently aliquoted and stored for use throughout all experimental procedures. Sebacic acid ($C_{10}H_{18}O_4$, SA, 99 %), epoxidized soybean oil ($C_{57}H_{98}O_{12}$, ES), and 4-dimethylaminopyridine ($C_7H_{10}N_2$, 99 %) were procured from Shanghai Macklin Biochemical Technology Co., Ltd. The chemicals used for laboratory preparation of melamine/epichlorohydrin prepolymer - including melamine ($C_3H_6N_6$)), epichlorohydrin (C_3H_5ClO), and sodium hydroxide (NaOH) - were also obtained from the same supplier. Poplar veneers (1.5 mm thickness) were provided by Wenan Wood Industry Co., Ltd. (Hebei, China). Ceramic and steel test specimens (100 × 25 mm) were custom-made by Dongfu Electronics Store (Guangdong). All solvents and reagents were used as received without further purification.

2.2. Preparation of epoxidized melamine prepolymer (EM)

For the preparation of EM in the laboratory, 10 g of melamine was first dissolved in 100 mL of deionized water. The solution was heated to 70 °C with continuous stirring until complete dissolution was achieved. Subsequently, 15 mL of epichlorohydrin was slowly added dropwise under stirring conditions, with the dropping rate carefully controlled to prevent localized overheating. Then, 0.5 g of NaOH was added as a catalyst, and the reaction system was heated to 80 °C. The reaction was maintained for 5 h with constant stirring, during which the pH was adjusted to 8–9 by adding dilute hydrochloric acid or sodium hydroxide solution as required (The detailed reaction equation is provided in Supporting Information S1). After completion of the reaction, the mixture was cooled to room temperature. Unreacted melamine was removed by filtration, and the product was washed three times with deionized water to eliminate residual catalyst and byproducts. Finally, the product was dried at 70 °C to constant weight to obtain solid EM [38]. All operations were conducted in a fume hood with appropriate personal protective equipment to ensure safety.

2.3. Preparation of ESS

Epoxidized soybean oil (ES) and sebacic acid (SA) at a mass ratio of 9:1, along with 0.5 % 4-dimethylaminopyridine (DMAP) as catalyst, were added to a three-neck flask. The reaction was carried out at 150 °C in a constant-temperature oil bath under mechanical stirring for 9 min. During the reaction process, the epoxy groups in ES and the carboxyl groups in SA underwent ring-opening esterification to synthesize hydroxyl-terminated polyester (ESS), which was obtained as a pale-yellow oily liquid.

2.4. Preparation of SM-based adhesives

SM-based adhesives were synthesized via a one-pot polymerization method using SM, ESS, and EM as raw materials. To ensure the homogeneity of the SME/ESS adhesives, SM and EM were first dissolved in deionized water and stirred thoroughly at 25 °C for 5 min. ESS was added to the SM-based adhesive at gradient concentrations of 5 wt%, 10 wt%, and 15 wt% by weight relative to the total composition and the mixture was stirred for an additional 5 min. The specific formulations are detailed in Table 1.ESS was then added, and the mixture was stirred for an additional 5 min, specific formulations are provided in Table 1. Through this straightforward procedure, a series of adhesives were successfully prepared.

Table 1
Components of the SM-based adhesives.

Sample	SM (g)	Water (g)	EM (g)	ESS (g)
PSM	30	70	0	0
SME	30	70	1.5	0
SME/5ESS	30	70	1.5	5.34
SME/10ESS	30	70	1.5	11.28
SME/15ESS	30	70	1.5	17.91

2.5. Mechanical testing

An adhesive quantity of 0.2 g was uniformly applied between two poplar veneers (bonding area: 25 × 25 mm). The assembly was then pre-pressed at 20 °C using a clamp (pressure: 1.0 MPa) for 1 h. Eight parallel samples were prepared using the same parameters (n = 8). After pre-pressing, the specimens were removed and subjected to pre-pressing shear strength testing using an AGS-X electronic universal testing machine (Shimadzu, Japan).

The designed SM-based adhesive was uniformly applied to both surfaces of the core layer in three-layer plywood (adhesive spread: 180 g/m^2). The adhesive-coated plywood was then placed in a hot press for processing. Hot-pressing parameters were set as follows: 320 s/mm, temperature maintained at 120 °C, and pressure at 1.0 MPa. Eight parallel samples were prepared using the same parameters ($n = 8$). After hot-pressing, the plywood samples were allowed to stand at room temperature for 24 h to ensure complete adhesive curing.

Twelve plywood specimens (100 × 25 mm) were prepared for performance evaluation. Six specimens were designated for dry-condition shear strength testing, while the remaining six were used for wet-condition testing. Wet-condition specimens were first immersed in a constant-temperature water bath at 63 ± 1 °C for 3 h, followed by 5 min at 25 °C to simulate practical service conditions. Prior to testing, all plywood specimens were conditioned at room temperature for 24 h. Shear strength testing was conducted using the AGS-X electronic universal testing machine (Shimadzu, Japan) at a crosshead speed of 10 mm/min. Ceramic, steel, and wood substrates (100 × 25 mm) were used to evaluate the adhesive's lap shear adhesion across different materials. A 0.2 g adhesive quantity was uniformly applied to the overlapping area (25 × 25 mm), followed by curing at 120 °C under 1 MPa pressure for 6 min. After 24 h of room temperature conditioning, the bonded assemblies were cut and subjected to lap shear testing.

The residual rate test was conducted by placing the adhered sample in an oven at 120 °C until a constant weight (Initial drying mass) was achieved to determine its residual rate. Subsequently, the sample was wrapped in filter paper and immersed in water at 60 °C for 6 h, followed by drying at 105 °C for 3 h until a constant weight (The quality after soaking in water and drying again) was attained. The remaining rate was calculated using the formula The quality after soaking in water and drying again / Initial drying mass (%). All experiments were repeated three times to ensure data reliability.

The adhesive sample was uniformly coated onto the surface of a glass slide and then placed in an oven at 120 ± 2 °C for curing, with a curing duration of 3 h to ensure complete drying of the adhesive. During the curing process, the sample was weighed every 30 min. If the mass change between two consecutive weightings was less than 0.5 %, the adhesive was considered fully cured, and the sample was removed. After cooling the adhesive to 25 °C, the morphology and performance of the cured adhesive layer were examined.

An experimental study on the mechanical stability performance was designed based on daily living scenarios. The stainless-steel sheet adhesive specimens were subjected to forceful impacts by an adult male, with strikes applied both frontally and laterally. Additionally, the specimens were dropped from a height of 1000 mm above a PVC-

surfaced table through free fall motion. The damage conditions of the adhesive joints were subsequently observed and analyzed.

Through the aforementioned testing methods, the pre-press performance, shear strength, lap shear adhesion, residual rate, toughness, and morphology of the cured adhesive layer of the SM-based adhesive were comprehensively evaluated, ensuring the reliability of the experimental data and the thorough assessment of the adhesive's properties.

2.6. Observation of the cured adhesive layer

The three-layer plywood was sectioned into 50 μm thin slices using an ultramicrotome (Leica EM UC7, Germany), and the penetration of the adhesive was observed using a Leica DM2500 optical microscope.

2.7. Physical properties testing

The fluidity of the liquid-modified soy protein adhesive was determined by Kinexus lab+ rheometer at a constant temperature of 25 °C. The adhesive was uniformly applied onto a parallel plate with a radius of 10 mm, maintaining a 1 mm gap between the rotor and the plate. The shear rate was gradually increased from 1 rpm to 60 rpm, and each adhesive sample was tested three times, with the average value recorded.

Under constant temperature and humidity conditions (25 °C, 60 % relative humidity), 15 g of the liquid adhesive sample was placed in a sterile Petri dish with a diameter of 4 cm. The mass of the adhesive residue was recorded at 12 h and 24 h intervals to evaluate its water retention capability.

The liquid adhesive was evenly applied onto the surface of poplar veneer using a coating rod. The spreading area of different adhesive samples was compared, and the residual adhesive on the rod was documented. The coating performance was recorded using a digital camera.

2.8. Basic characterization

The adhesive sample was placed in a drying oven at 120 ± 2 °C for curing until no further weight change was observed, indicating completion of the curing process. Subsequently, the cured adhesive was ground into a homogeneous powder, ensuring it could pass through a 200-mesh sieve. The obtained adhesive powder was mixed with potassium bromide (KBr) at a predetermined ratio and pressed into a transparent film using a mold for Fourier transform infrared spectroscopy (FT-IR) testing, aiming to analyze the chemical composition, functional groups, and chemical bond structure of the SM-based adhesive.

The surface and internal microstructure characteristics of the cured SM-based adhesive were examined by scanning electron microscopy (SEM) to evaluate its morphology and structural uniformity. X-ray diffraction (XRD) was employed to analyze the internal crystal structure of the SM-based adhesive, providing further insight into its crystalline behavior. Thermogravimetric analysis (TGA) was conducted to assess the thermal stability of the cured adhesive, analyzing its mass change and decomposition behavior at different temperatures.

Furthermore, X-ray photoelectron spectroscopy (XPS) was utilized for elemental composition analysis of the sample, with Al-Kα radiation ($h\nu = 1486.6$ eV) at a resolution of 0.1 eV, to investigate changes in elemental composition during the curing process. To further observe the microscopic morphology of the adhesive, the cured adhesive block was sputter-coated with gold and then subjected to high-resolution imaging using a cold-field emission scanning electron microscope (SEM, Regulus 8100, Japan) at an accelerating voltage of 10 kV, revealing detailed features of its microstructure.

2.9. Life-cycle assessment

The environmental impact assessment modeling of the adhesive was conducted using OpenLCA 1.11.0 software, with the US Life Cycle Inventory (USLCI) database and Ecoinvent 3 database, along with TRACI (version 2.1). The functional unit for the LCA in this study was defined as "the production of 1 kg of adhesive".

2.10. Mildew resistance test

Fifteen grams of liquid soybean protein adhesive sample was placed in a 4 cm sterile plastic Petri dish and maintained in a constant temperature and humidity incubator at 30 °C and 90 % relative humidity, three parallel sterile petri dishes ($n = 3$) were prepared for each formula for testing. The mold growth on the adhesive surface was recorded every 24 h using a digital camera. The liquid adhesive was dried at 120 °C until a constant mass was achieved. The plywood samples coated with the adhesive were then placed in a constant temperature and humidity incubator at 35 °C and 100 % relative humidity, and mold growth was recorded every 2 days.

2.11. Flammability test

Each adhesive sample was uniformly applied to one side of the plywood. The adhesive-coated surface was exposed to an alcohol lamp flame for 10 s. The burning behavior of the adhesive and its flame-retardant protective effect on the covered plywood surface were observed to evaluate the flammability of the adhesive.

3. Results and discussion

3.1. The design, fabrication and structural characteristics of SM/ESS adhesives

To construct a spider silk-inspired cured adhesive structure, the crosslinking agent EM was first reacted with the active groups of soybean protein Fig. 1a. Subsequently, polyester ESS, synthesized from epoxidized soybean oil (ESO) and sebacic acid, was introduced into the adhesive system as a buffer layer to dissipate stress. The preparation flowchart is illustrated in Fig. 1b. The comparative FT-IR spectra of ES and ESS are shown in Fig. 1d. The red stripe (~823 cm^{-1}) points to a very distinct and characteristic absorption peak in the spectrum of epoxidized soybean oil (ESO), which is attributed to the symmetric stretching vibration of the epoxy group (C-O-C). Its presence indicates that the ESO raw material contains abundant epoxy functional groups. The blue stripe (~1684 cm^{-1}) points to a newly emerged absorption shoulder in the spectrum of the hydroxyl-terminated polyester (ESS), which is attributed to the stretching vibration of the C═O bond in the ester group (-COO-). The appearance of this peak is direct evidence that the ring-opening esterification reaction between epoxy groups and carboxyl groups has occurred, resulting in the formation of ester bonds. The FT-IR analysis of different adhesives (Fig. 1e) revealed that the characteristic absorption peaks of peptide bonds in the SM adhesive exhibited typical secondary structure features of proteins. A strong absorption peak at 1650 cm^{-1} was assigned to the amide I band, primarily arising from the C═O stretching vibration of peptide bonds. The peak at 1534 cm^{-1} corresponded to the amide II band, reflecting the coupling mode of N—H bending and C—N stretching vibrations. Meanwhile, the peak at 1238 cm^{-1} was attributed to the amide III band, representing a combination of C—N stretching and N—H in-plane bending vibrations. These characteristic peaks confirmed the presence of intact peptide bond structures in the adhesive system, providing critical structural evidence for subsequent studies on intermolecular interaction mechanisms. Upon the addition of the crosslinking agent EM, a new absorption peak emerged at 1747 cm^{-1}, characteristic of the carbonyl group, indicating the crosslinking reaction between EM and the active groups of soybean protein, forming a rigid adhesive structure. The appearance of a peak at 769 cm^{-1} confirmed the out-of-plane bending vibration of the triazine ring, demonstrating the uniform dispersion of EM in the protein

adhesive system. After ESS modification, the adhesive system formed a more stable composite structure, as evidenced by the blue shifts of the amide I, II, and III bands to 1690, 1548, and 1252 cm^{-1}, respectively. Additionally, newly emerged peaks at 1241, 1744, and 2854 cm^{-1} were assigned to C—O asymmetric stretching vibration, polyester carbonyl characteristic peak, and aliphatic C—H stretching vibration, respectively, indicating uniform dispersion of ESS in the system. Furthermore, the O—H characteristic peak exhibited a blue shift to a lower wavenumber (3273 cm^{-1}), suggesting enhanced hydrogen bonding interactions in the adhesive system. These results demonstrate that the rigid protein network formed by EM crosslinking, combined with ESS introduced via hydrogen bonding as a buffer layer for energy dissipation, collectively constitutes a protein adhesive system with balanced rigidity and flexibility.

XPS (X-ray Photoelectron Spectroscopy) measures the energy distribution of photoelectrons emitted from a material surface upon X-ray excitation, providing information on elemental composition, chemical states, and electronic structure. As revealed by XPS analysis (Fig. 2a-f), significant changes in the chemical structure were observed between PSM and SME/10ESS. In the N1s spectrum of SME/10ESS, the peak area corresponding to N—H was reduced, while that of the C—N bond increased. This phenomenon indicates that the amino groups in the protein molecules reacted with the crosslinking agent. In the C1s spectrum of the SME/10ESS adhesive, the peak area of the C—C bond was significantly enhanced, suggesting the formation of a more densely crosslinked and cured structure. Additionally, the C═O peak shifted from 288.2 eV to 289.0 eV, and a new peak appeared at 286.3 eV. Concurrently, in the O1s spectrum, the C═O peak shifted from 533.0 eV to 533.4 eV. These changes demonstrate the reorganization of the chemical states of carbon and oxygen atoms in the material. These results reveal the chemical structural alterations in the adhesive, which are consistent with the FT-IR characterization.

X-ray diffraction (XRD) characterizes the crystal structure, phase composition, and microstructural parameters of materials by analyzing their X-ray diffraction patterns. In this study, XRD analysis revealed that PSM exhibited characteristic diffraction peaks at $2\theta = 8.31°$ and 19.79°, corresponding to α-helix and β-sheet structures, respectively (Fig. 2g). Specifically, the diffraction peaks of PSM at 8.31° and 19.79° should more accurately be attributed to a certain aggregated state structure with a degree of regularity, formed through interactions such as hydrogen bonding between protein molecules. After the construction of the bioinspired structure by the introduction of EM and ESS, the shifts and intensity changes observed in these characteristic diffraction peaks essentially indicate that the original stacking mode of the soy protein

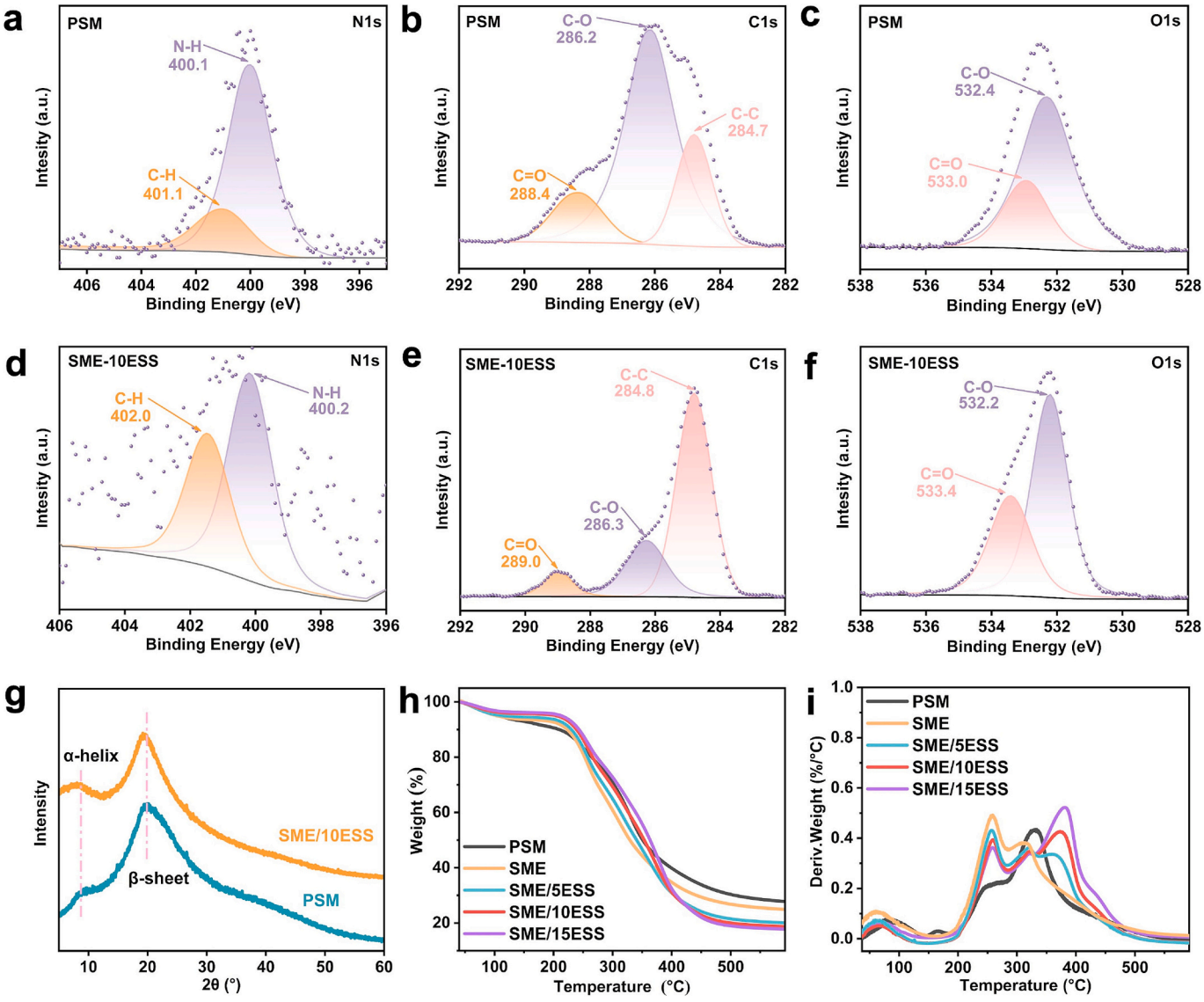

Fig. 2. (a-f) XPS spectra of SM-based adhesives; (g) Comparative XRD spectra of PSM and SME/10ESS adhesives; (h,i) TG and DTG curves of SM-based adhesives.

was disrupted by the bioinspired structure constructed in the adhesive system, leading to a decrease in crystallinity and an increase in crosslinking density. This change in the aggregated state structure is fully consistent with the variations in protein secondary structure observed by FT-IR. Together, they demonstrate the profound influence of the bioinspired structure on the molecular architecture of the protein system. This observation indicates a substantial change in the secondary structure of the protein, where the original ordered helical and folded conformations were partially disrupted, and the crystallinity of the cured adhesive decreased. These structural evolutions can be attributed to two factors: on one hand, the crystalline regions in SM formed a crosslinked network during the curing process; on the other hand, the incorporation of ESS not only densified the adhesive structure but also enhanced the material's toughness by constructing stress-transfer channels.

3.2. Performances of the of SM/ESS adhesives

The water retention property of an adhesive is one of the key factors influencing its processing performance and final bonding quality. Good water retention ensures that the adhesive maintains an appropriate viscosity during application, preventing coating difficulties caused by excessive water evaporation. It also preserves sufficient open time, allowing adequate wetting and penetration of the bonded materials, while ensuring thorough internal curing of the adhesive layer and avoiding incomplete curing or internal stress concentration due to premature water loss. The water retention performance of the adhesives was tested under constant temperature and humidity conditions (25 °C, 60 % relative humidity) (Fig. 3a). After 24 h of observation, distinct differences in water retention were observed among the different adhesive formulations, reflected in variations in shrinkage rate and cracking degree. The experimental results demonstrated significant differences in water retention capability among the samples. Under the test conditions, PSM and SME adhesives retained residual mass percentages of 46.2 % and 48 %, respectively. However, upon the introduction of ESS into the adhesive system, the water retention performance was significantly improved, maintaining over 60 % mass retention after 24 h, with SME/10ESS adhesive achieving a residual mass retention rate of 67.3 % (Fig. 3c). This performance enhancement is primarily attributed to the presence of polar functional groups such as ester bonds and hydroxyl groups in the ESS molecular chains, which can form hydrogen bonds with water molecules, thereby delaying evaporation. Additionally, the long-chain aliphatic structures in the polyester may form hydrophobic microdomains that hinder the continuous-phase diffusion of water, while the hydrophilic groups still allow localized water retention within these regions. These factors collectively slow down the migration of water molecules from the interior to the surface of the adhesive, reducing water evaporation and effectively improving water retention. This improvement holds significant practical value for enhancing production efficiency and bonding stability.

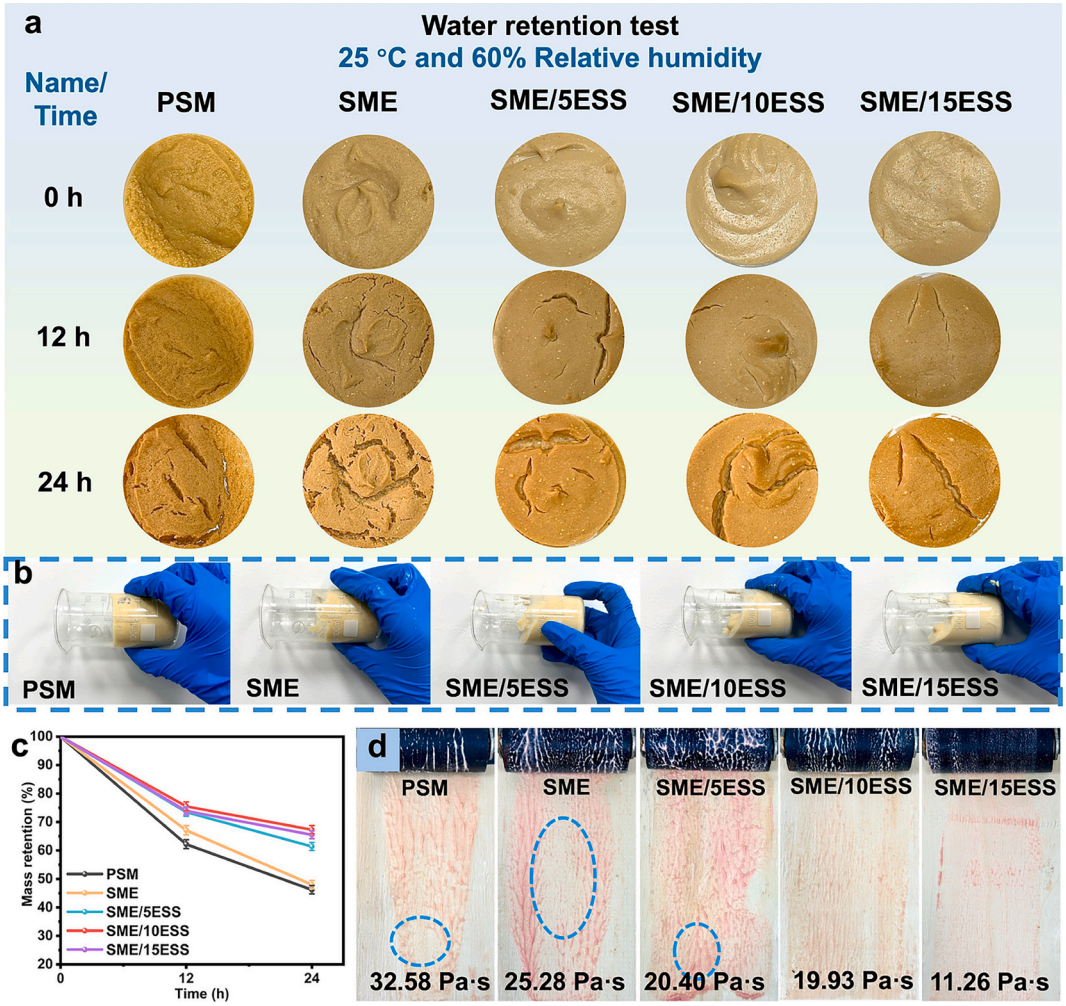

Fig. 3. Water retention performance and viscosity of the adhesive. (a) The surface shrinkage and cracking of the five adhesives after being stored under certain conditions for 24 h; (b) Photos of the fluidity of different adhesives; (c) The mass of soy protein-based adhesive stored at 25 °C and 50 % RH for 24 h; (d) The coating performance of the adhesive on wood.

In wood processing, the coating performance of adhesives plays a crucial role in determining the bonding quality and long-term stability of the final product. Only when an adhesive possesses good fluidity can it be uniformly distributed on the wood surface and sufficiently wet the substrate, thereby achieving strong bonding strength (Fig. 3b). Experimental results showed that the viscosity of unmodified soybean protein adhesive was 32.58 Pa·s. After the addition of EM, the viscosity of the adhesive decreased by 22.4 % to 25.28 Pa·s. When the ESS content was gradually increased from 5 % to 15 %, the adhesive viscosity decreased from 20.40 to 11.26 Pa·s. By constructing a biomimetic structure in the adhesive system, the viscosity of SME/10ESS adhesive was reduced by 38.8 % to 19.93 Pa·s compared to the PSM adhesive. This change significantly improved the fluidity of the adhesive on the substrate, primarily due to the introduction of small molecules into the adhesive system through biomimetic structuring, which acted as molecular lubricants, effectively reducing the viscosity and wettability of the protein adhesive. Furthermore, the modified adhesive exhibited a notable improvement in coating performance. Moreover, the staining method was adopted to visually compare the coating uniformity and application performance of different adhesive formulations on poplar veneer (as shown in Fig. 3d). The unmodified PSM adhesive, due to its high viscosity and poor fluidity, exhibited uneven coating and significant residue after staining. In contrast, the modified SME/10ESS adhesive showed uniform dye distribution and minimal residue, which is consistent with its significantly reduced viscosity (19.93 Pa·s) and improved rheological data (Fig. 3b). Such uniform distribution facilitates the formation of a stable and continuous bonding layer, which is highly beneficial for improving the bonding quality and strength of wood.

To meet the requirements of handling and repair processes during the production of bonded products, the adhesive layer between veneer substrates is required to possess good prepressing performance to enhance production line efficiency. Therefore, the prepressing performance of adhesives serves as one of the critical parameters for evaluating the production efficiency of bonded products. The prepressing strength test results of plywood demonstrated that the unmodified protein adhesive exhibited a prepressing strength of only 0.18 MPa, which failed to maintain bonding performance during production line processing, leading to poor stability and a high risk of veneer separation, thus being unsuitable for industrial processing requirements (Fig. 4e). However, after the protein adhesive was reinforced through biomimetic structure construction, the SME/10ESS adhesive achieved a prepressing strength of 0.78 MPa for the prepared plywood, representing a 333.3 % improvement. This enhancement meets practical application requirements, effectively reduces the risk of veneer separation during transportation, and improves both bonding stability and production line efficiency.

The residual rate of the adhesive can directly reflect its water

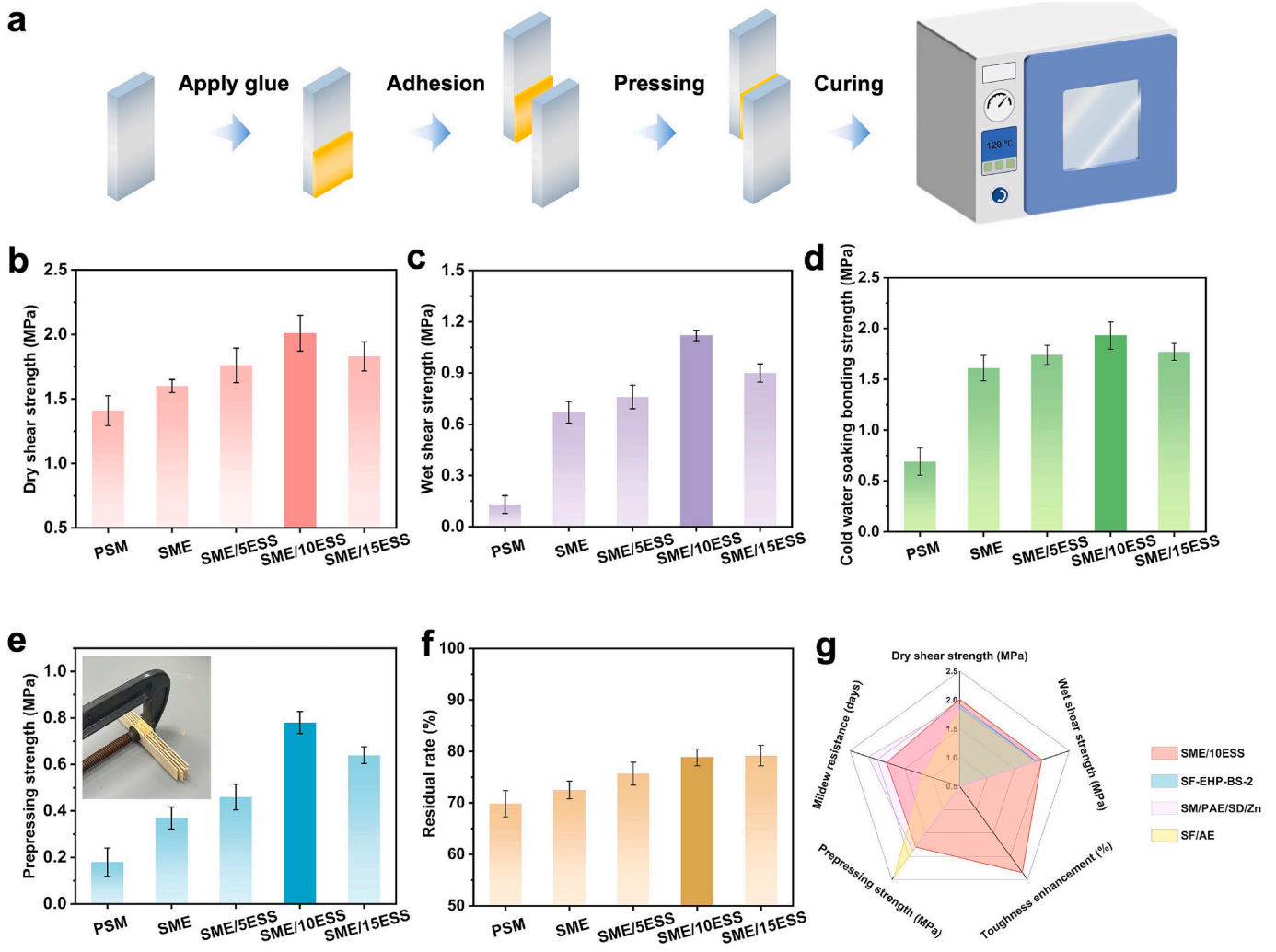

Fig. 4. (a) Schematic diagram of the steps for bonding wood with adhesive; (b, c) Dry/wet shear strengths of SM-based adhesives with different amounts of ESS added; (d) Shear strength of various adhesives when soaked in cold water; (e) The preloading strength of the adhesive; (f) Comparison chart of residue rates of various adhesives; (g) Radar chart compared with the reported adhesives.

resistance. Due to its loose cross-linked network and abundant hydrophilic groups, the PSM adhesive exhibited a residual rate of only 69.85 % (Fig. 4f). In contrast, the SME/10ESS adhesive showed a significantly improved residual rate of 78.84 %. This enhancement was attributed to the covalent cross-linked network formed by the reaction between EM and the active groups of soybean protein, while the introduction of ESS through hydrogen bonding further densified the cross-linked structure, effectively improving resistance to water molecule penetration and thus enhancing water resistance. The potential of soybean meal adhesive for high-performance applications and the key factors influencing its shear performance were investigated through the analysis of plywood shear strength. The dry shear strength of the PSM adhesive was 1.41 MPa (Fig. 4b). However, after 3 h of cold-water immersion, its strength decreased to 0.69 MPa, and after 3 h of hot-water (63 °C) immersion, the wet shear strength further dropped to 0.31 MPa (Fig. 4c). These results indicate the poor water resistance of the unmodified adhesive, severely limiting the practical performance of plywood. Upon the addition of the cross-linking agent EM, which reacted with the active groups of soybean protein to form a covalent cross-linked network, the dry shear strength of plywood prepared with SME adhesive increased by 13.4 % to 1.6 MPa. The cold-water immersion shear strength improved by 133.3 % to 1.61 MPa, while the hot-water immersion shear strength increased to 0.67 MPa (Fig. 4d). Further introduction of ESS to construct a biomimetic structure resulted in additional improvements. The SME/5ESS adhesive exhibited a dry shear strength of 1.76 MPa, a cold-water immersion shear strength of 1.74 MPa, and a hot-water immersion shear strength of 0.76 MPa (a 145.2 % increase). With an optimal increase in ESS content, the SME/10ESS adhesive achieved a dry shear strength of 2.01 MPa (a 42.6 % increase), a cold-water immersion shear strength of 1.93 MPa (a 179.7 % increase), and a hot-water immersion shear strength of 1.12 MPa (a 261.3 % increase). However, when the ESS content was further increased to 15 %, the shear strength of the plywood slightly decreased by 9.0 % and 20.0 % under dry and hot wet conditions, respectively, to 1.83 MPa and 0.90 MPa. This was attributed to the excessively low viscosity of the SME/15ESS adhesive, which led to excessive penetration into wood pores, causing glue starvation and preventing the formation of an effective adhesive layer, thereby reducing bonding strength. By constructing a biomimetic structure in the adhesive system, not only were the mechanical properties of the adhesive enhanced in high-humidity environments, but its stability in practical applications was also significantly improved.

The changes in the work of adhesion for various adhesives were analyzed by calculating the integral area under the force-displacement curves obtained from wet shear strength tests (Fig. 6j). The debonding work of PSM adhesive was only 0.072 J, indicating extreme brittleness after curing. Compared with PSM, the work of adhesion for SME/10ESS adhesive increased by 212.5 % to 0.225 J. The SME/15ESS adhesive exhibited a 344.4 % improvement in work of adhesion, rising from 0.072 J to 0.32 J. The failure strain increased from 0.36 mm to 0.83 mm, demonstrating enhanced toughness of the SME/15ESS adhesive, which facilitated more effective stress transfer and energy dissipation under external loading. Furthermore, the variation in toughness was characterized by observing the fracture patterns of cured adhesive films (Fig. 6i). In spider silk, the dense crystalline regions provide high strength, while the loose amorphous regions serve as buffer layers to relieve stress, endowing the material with both strength and toughness.

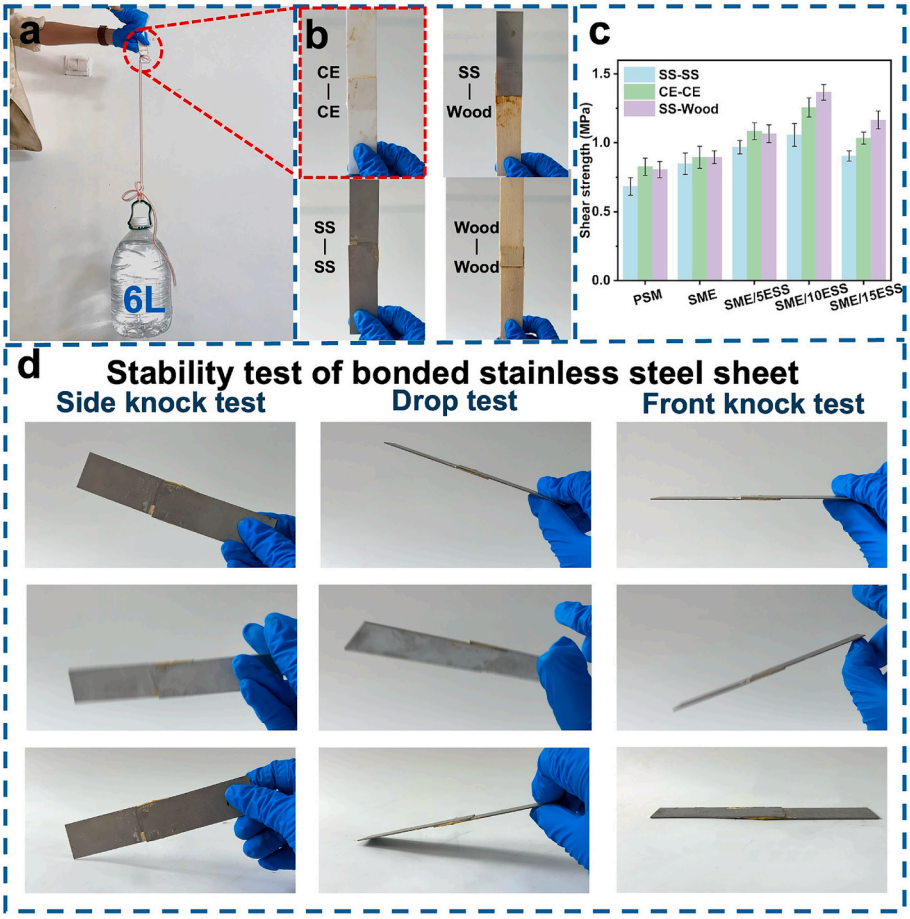

Fig. 5. (a) The SME/10ESS adhesive bonded ceramic sheet can vertically lift a water bottle containing 6 L of water; (b) Photos of SME/10ESS adhesive bonding various substrates; (c) Shear strength of adhesives for bonding different materials; (d) Stability tests of bonded steel sheets: side knock test, drop test and front knock test.

Similarly, in the biomimetic adhesive system, a rigid network was formed through cross-linking reactions between EM and the active groups of soybean protein, while ESS was introduced as a buffer layer through hydrogen bonding to relieve stress and dissipate energy, effectively improving the toughness of the adhesive.

Through the construction of a biomimetic network structure, the SME/10ESS adhesive demonstrates outstanding mechanical properties. This adhesive is not only suitable for wood bonding but also enables effective bonding between homogeneous or heterogeneous materials such as ceramic (CE) and stainless steel (SS) (Fig. 5b). However, the differences in adhesive strength observed among ceramic, stainless steel, and wood substrates are fundamentally attributed to their distinct surface physical and chemical characteristics. Wood is a natural porous material, and wood veneer surfaces are rich in polar functional groups such as hydroxyl groups (-OH). The SME/10ESS adhesive used in this study contains abundant polar groups, including amino, hydroxyl, and ester groups. Therefore, the excellent interfacial strength is primarily influenced by two factors. Firstly, during the pre-pressing and hot-pressing processes, the adhesive can penetrate the pores and cell cavities of the wood, and after curing, it forms a powerful "mechanical interlocking" effect. Secondly, dense hydrogen bond interactions can be formed between the adhesive molecules and the surface molecules of the wood. These two interactions contribute to the strong adhesive strength of the adhesive on wood. The surface of stainless steel is relatively smooth and non-porous but is typically covered by a natural oxide layer, which provides polar sites such as hydroxyl groups. The main interactions with this surface are van der Waals forces and dipole–dipole interactions. The strength of these adsorptive forces is generally lower than the synergistic effect of mechanical interlocking and hydrogen bonding in wood, which may explain its slightly lower adhesive strength. The ceramic surface is highly polar and rich in hydroxyl groups; however, its structure is dense with low porosity, making mechanical interlocking almost unachievable. Therefore, adhesion mainly relies on hydrogen bonding and ion–dipole interactions formed between the polar groups in the adhesive and the ceramic surface. The strength is relatively slightly lower than that on wood, precisely due to the lack of contribution from macroscopic mechanical anchoring.

Furthermore, it was intended to visually demonstrate the mechanical performance of the adhesives through an intuitive test. The bonded stainless-steel specimens were struck with force by an adult male, including impacts from both the front and side. Additionally, the specimens were dropped from a height of 1000 mm above a desktop through free fall onto a PVC desktop, and the bonded area (25 × 25 mm) of the stainless-steel specimens adhered with the SME/10ESS adhesive remained intact, with no failure observed. (Fig. 5d). Moreover, ceramic specimens bonded with this adhesive could stably support the weight of a 6 L water bottle without detachment (Fig. 5a). These exceptional mechanical properties originate from the synergistic effect of ESS and EM, which forms a biomimetic network structure in the adhesive system capable of effectively dissipating external impact energy (Fig. 5c).

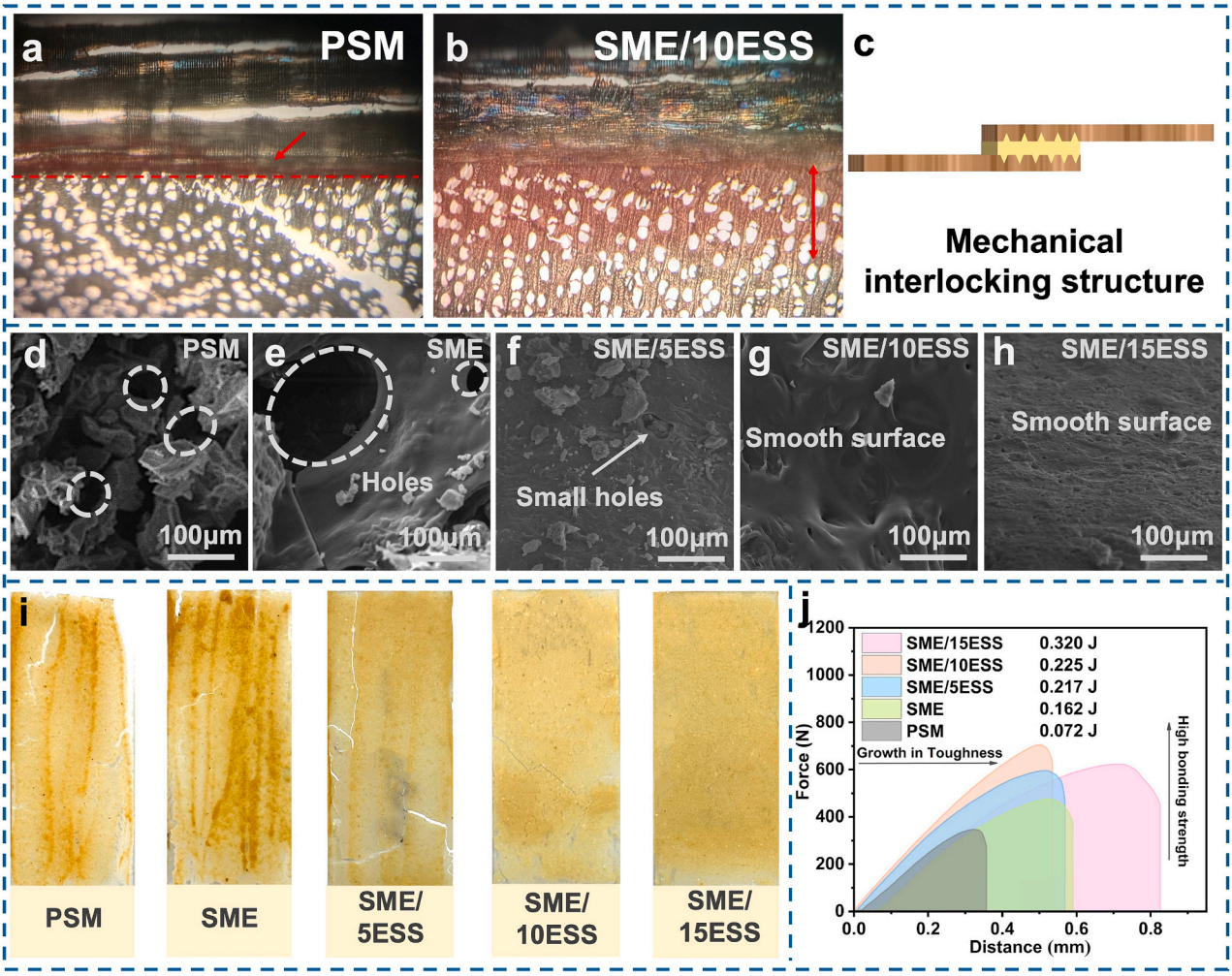

Fig. 6. (a, b) Observation of the adhesive lines for bonding plywood with PSM and SME/10ESS adhesives; (c) Schematic diagram of the mechanical interlocking structure formed between SME/10ESS adhesive and wood substrate; SEM image of the fracture surface of (d-h) adhesive samples; (i) Observation of cracks in different cured adhesive films; (j) Force–displacement curve of shear strength after soaking in warm water (63 °C).

Experimental evidence confirms that the superior adhesive performance of SME/10ESS adhesive holds promising application prospects in industrial fields such as wood processing and ceramic restoration.

3.3. Micromorphology of SM/ESS adhesives

The microscopic morphology of the plywood cross-section interface and adhesive penetration were analyzed. The upper portion of the images shows the transverse section of poplar veneer, revealing typical wood microstructures including rays, vessels, and fibers, while the lower portion displays the radial section of the veneer. The results indicate that due to its high viscosity and poor fluidity during hot-press curing, the PSM adhesive exhibited weak penetration capability into the wood substrate (Fig. 6a-b). This limited penetration depth failed to establish an effective mechanical interlocking structure with the wood substrate, resulting in poor bonding strength (Fig. 6c). In contrast, after the construction of a biomimetic structure, the SME/10ESS adhesive demonstrated effective penetration to a depth of 2–3 cell layers beneath the wood surface, forming adhesive nails. This significantly enhanced the interfacial bonding force between the adhesive and wood, thereby improving the bonding performance of the final product.

Surface morphology observation can directly reveal the microstructural characteristics of adhesives, providing key evidence for understanding their bonding mechanisms. As shown in Fig. 6d, the PSM adhesive surface exhibits obvious pores of varying sizes and a relatively rough texture. This loose microstructure is susceptible to moisture penetration, resulting in poor water resistance and mechanical properties. After the incorporation of crosslinking agent EM into the system, pores and cracks are still observed on the surface, but their number and size are reduced, indicating a denser structure. With the introduction of ESS into the adhesive system and increasing its content, the surface morphology of the cured adhesive gradually changes from rough and porous to smooth, with significantly reduced pores or cracks (Fig. 6e-h). This improvement contributes to enhanced bonding performance and appearance quality of the adhesive. These observations demonstrate that through the construction of a biomimetic structure by introducing EM and ESS, the cured adhesive structure becomes more compact and uniform. This effectively enhances the cohesive strength of the soybean protein adhesive and improves its resistance to moisture penetration, thereby increasing the water resistance of the cured adhesive.

3.4. Thermal properties and flame retardancy analysis

The thermal stability, decomposition temperature and component changes of soybean protein adhesives were characterized by TG and DTG. The SM-based adhesive exhibited three distinct weight loss stages during thermal degradation. The first stage (room temperature to 220 °C) was mainly attributed to the decomposition of free water, bound water and small molecular substances in the system. The second stage (220–350 °C) corresponded to the breakage of soybean protein side chain groups (such as polysaccharides and fatty acid segments) and unstable ester bonds in polyester. The third stage (350–500 °C) reflected the thermal decomposition of soybean protein backbone substances. However, the SME/ESS adhesives showed two degradation peaks in DTG analysis. Due to the presence of ester bonds in ESS, these bonds might begin to break at relatively low temperatures, releasing low molecular weight acids and alcohols, thus forming the first degradation peak. With increasing ESS content, the thermal stability of modified soybean protein adhesives was significantly improved, especially in the high temperature region above 350 °C. DTG analysis results (Fig. 2i) showed that compared with SM adhesive (330.2 °C), the maximum mass loss temperature of SME/10ESS adhesive with biomimetic structure increased to 374.2 °C. Meanwhile, the temperature corresponding to 50 % mass loss of cured SME/10ESS adhesive (352.5 °C) was higher than that of the PSM adhesive (347.3 °C) (Fig. 2h). This improvement in thermal stability originated from the biomimetic network structure formed by the introduction of EM and ESS, which could construct a denser adhesive layer and effectively inhibit heat and flammable gas transfer. These results demonstrate that the construction of biomimetic network structure significantly enhanced the thermal stability of the adhesive system. The residual char yield is a key indicator for evaluating the thermal stability of a material. The residual char yields for PSM, SME, SME/5ESS, SME/10ESS, and SME/15ESS were determined to be 18.7 %, 21.5 %, 23.8 %, 25.4 %, and 26.9 %, respectively (Fig. S5). This data trend clearly demonstrates that the residual char yield of the bio-inspired adhesive is significantly increased with the introduction and increasing content of ESS. The improvement in residual char yield is primarily attributed to the construction of a strong, tough, and dense bio-inspired adhesive system. The ESS within the system, as a bio-based polyester, undergoes cross-linking and char-forming reactions of its molecular chains at high temperatures. Furthermore, the dense cured bio-inspired structure effectively suppresses the release of volatile small molecules during pyrolysis and promotes the formation of a protective char layer, thereby enhancing the mass retention at high temperatures.

As proteins are biological macromolecules composed of amino acids linked by peptide bonds, their main elements include carbon, hydrogen, oxygen, nitrogen and sulfur. The presence of these elements enables proteins to undergo oxidation reactions during combustion, making them combustible (Fig. 7a). As shown in Fig. 7b, numerous pores and cracks were observed on the surface of PSM adhesive after combustion, resulting in a significantly roughened surface structure. This change may be attributed to the thermal decomposition of soybean protein at high temperatures, which damaged the internal structure of the material and led to the formation of more pores and cracks. In contrast, although some pores were also present on the surface of SME/10ESS adhesive after combustion, the overall structure remained relatively intact with fewer pores and a smoother surface (Fig. 7d). These results indicate that the adhesive containing ESS exhibits better thermal stability and could reduce the flammability of wood at high temperatures. During combustion, ESS forms a stable carbonized layer that can isolate oxygen and reduce heat transfer, thereby inhibiting combustion. To further investigate the ability to reduce flammability, they were uniformly coated on both sides of plywood and subjected to combustion tests after high temperature curing to observe their protective performance on poplar veneer substrates. Although SM adhesive showed relatively improved the ability to reduce flammability, localized carbonization at the substrate edges could still be observed after the adhesive layer was removed. When a biomimetic structure was constructed in the adhesive, a denser and more uniform cross-linked network structure was formed. Compared with the loose cured structure of PSM, this structure exhibited better protective performance. Moreover, ESS could form a stable carbonized layer at high temperatures, which isolated oxygen and reduced heat transfer, thereby suppressing combustion. Therefore, as shown in Fig. 7e, the poplar surface coated with SME/ESS adhesive exhibited a small, carbonized area, demonstrating excellent ability to decrease flammability.

3.5. Mildew resistance properties

Due to its rich content of proteins and polysaccharides, SM adhesive is highly susceptible to microbial erosion in humid and hot environments, which severely affects its bonding performance and product durability. In this study, accelerated mold growth experiments (30 °C/90%RH) were conducted to evaluate the mold resistance of different adhesive formulations (Fig. 8a). Experimental data showed that unmodified PSM adhesive exhibited obvious spoilage within 3 days, accompanied by unpleasant odors, indicating poor mold resistance. In contrast, after biomimetic modification, SME/10ESS adhesive demonstrated excellent anti-mold properties, with its shelf life extended to over 12 days. Table S2 summarizes the calculation results of the anti-mold area in each region and the mold growth rate, clearly indicating that SM/10ESS (12 days) had a moldy area proportion of only 16.20 %,

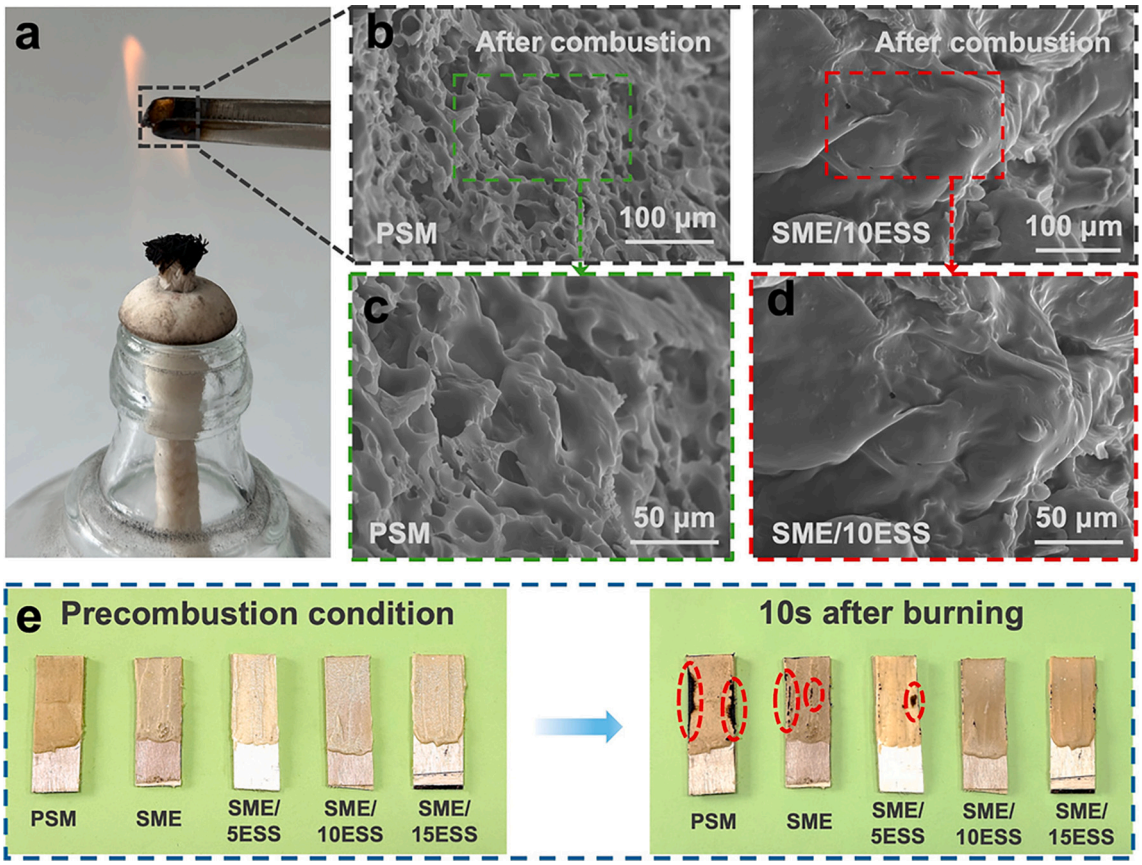

Fig. 7. (a) The glue block after the alcohol lamp burns and cures; (b-d) SEM images of PSM and SME/10ESS adhesives after combustion; (e) Experimental photos of the front side of wood after the SM-based adhesive was coated on the wood surface and the adhesive surface was burned with an alcohol lamp.

significantly lower than that of unmodified PSM (19.17 % at 3 days and 26.18 % at 12 days). Furthermore, SM/15ESS (12 days) showed an even lower moldy area proportion of 5.70 %, highlighting the effectiveness of ESS in enhancing mold resistance. This improvement was attributed to the hydrophobic long-chain fatty acid ester segments in ESS, which may disrupt the lipid bilayer structure of mold cell membranes, causing leakage of cellular contents and inhibiting mold growth. Additionally, the epoxy and ester groups in ESS's chemical structure possess certain antibacterial properties that can suppress mold proliferation (Fig. 8b). After 1 day of storage, the shear strength of plywood prepared with biomimetically modified SME/10ESS adhesive decreased by approximately 10.6 % to 1.01 ± 0.2 MPa. Even after 3 days of storage, the shear strength was reduced by merely 42.2 % to 0.71 ± 0.3 MPa. This study demonstrates that constructing a biomimetic structure in the adhesive system through the introduction of EM and ESS can significantly enhance the mold resistance of bio-based adhesives. The findings provide both theoretical foundations and technical pathways for developing long-term stable and environmentally friendly adhesive systems, which hold important practical significance for extending the service life of wood-based composites.

4. Conclusion

Spider silk is characterized by densely packed crystalline regions and loosely arranged amorphous regions, where the amorphous regions serve as buffer layers to relieve stress and dissipate energy, forming a strong and tough structural system. Inspired by this robust architecture, a rigid cross-linked network was constructed in this study through the reaction of an EM crosslinker with active groups on soybean protein, while a flexible polyester ESS was introduced into the adhesive system via hydrogen bonding as a stress-absorbing layer to mitigate impact and dissipate strain. Compared to unmodified soybean protein adhesive, the prepressing strength of SME/10ESS adhesive was increased to 0.78 MPa (a 333.3 % improvement) after incorporation of the biomimetic structure. Under dry and wet conditions, the shear strength reached 2.01 MPa and 1.12 MPa, representing increases of 42.6 % and 261.3 %, respectively. The work of adhesion was enhanced by 212.5 % to 225 mJ, indicating significantly enhanced toughness. Moreover, the biomimetically modified adhesive demonstrated broad applicability across various substrates and exhibited excellent water resistance, suggesting its potential for use in wood processing, ceramic restoration, and related fields. Coating performance was also improved, with viscosity reduced by 62.1 % to 19.93 Pa·s. The biomimetic modification was also found to significantly enhance mold resistance, enabling freshly prepared adhesive to remain mold-free for 12 days under the humidity conditions. LCA results demonstrate the environmental friendliness and sustainability of the adhesive (Fig. 1f). This biomimetic design strategy not only provides a new theoretical foundation for the development of versatile bio-based adhesives but also offers important technical support for promoting the green transformation of the traditional adhesive industry. However, the development of more efficient and cost-effective synthesis pathways for bio-based polyesters, the execution of pilot-scale validation to assess the feasibility of scale-up engineering techniques, and further investigation into the long-term durability of this adhesive under extreme environments remain to be thoroughly investigated.

CRediT authorship contribution statement

Guoyan Zuo: Conceptualization. **Feng Zhu:** Methodology. **Guodong Zeng:** Investigation. **Ying Zhou:** Conceptualization. **Jiongjiong Li:** Conceptualization. **Qiang Gao:** Writing – review & editing. **Jing Luo:** Writing – review & editing. **Zeli Que:** Writing – review & editing.

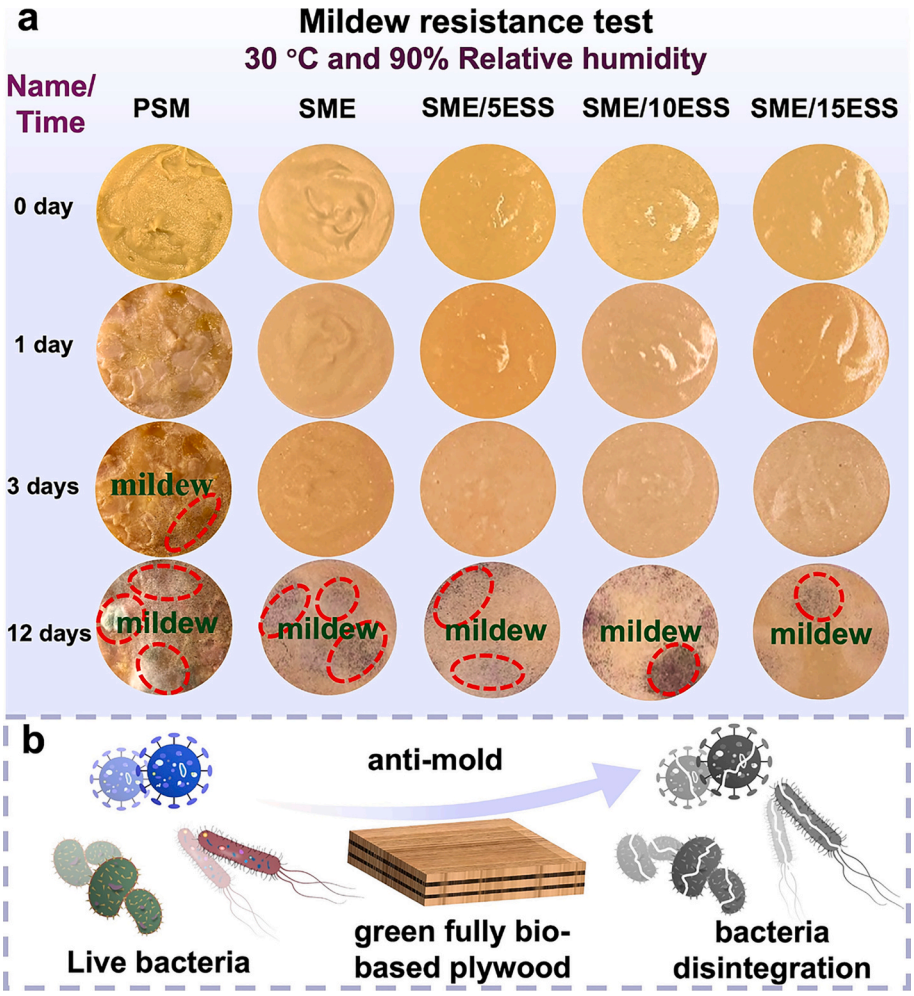

Fig. 8. (a) Anti-mold properties of different adhesives under constant temperature and humidity; (b) Schematic diagram of mold prevention for SME/ESS adhesive.

Jianzhang Li: Writing – review & editing.

Declaration of competing interest

The authors declare that they have no known competing financial interests or personal relationships that could have appeared to influence the work reported in this paper.

Acknowledgments

This work was financially supported by National Key Research and Development Program of China during the 14th Five-Year Plan Period (2024YFD2201204).

Appendix A. Supplementary data

Supplementary data to this article can be found online at https://doi.org/10.1016/j.ijbiomac.2025.148756.

Data availability

No data was used for the research described in the article.

References

[1] Z. Jiang, S. Zu, C. Li, J. Pang, Research progress on lignin-based epoxy resins: a green and sustainable path from biomass to new materials, Polym. Eng. Sci. (2025), https://doi.org/10.1002/pen.70114.

[2] G. Yang, Z. Gong, X. Luo, L. Chen, L. Shuai, Bonding wood with uncondensed lignins as adhesives, Nature 621 (7979) (2023) 511–515, https://doi.org/10.1038/s41586-023-06507-5.

[3] Q. Zhu, R. Li, Y. Yan, Y. Huang, H. Su, Y. Dong, X. Pan, W. Sun, X. Wang, H. Meng, R. Wang, H. Ouyang, Y. Hong, Sustainable snail-inspired bio-based adhesives with ultra-high adhesion, Adv. Funct. Mater. 34 (38) (2024), https://doi.org/10.1002/adfm.202402734.

[4] R. Yan, Q. Zhang, D. Wu, M. Hou, X. HongLei, H. Zhou, G. Essawy, A. Du, X. Xi Pizzi, Preparation and analysis of environment-friendly and high- performance cellulose-based wood adhesive, Int. J. Biol. Macromol. 304 (Pt 1) (2025) 140642, https://doi.org/10.1016/j.ijbiomac.2025.140642.

[5] L. Chen, J. Qian, C. Xu, Z. Liu, W. Han, X. Ji, Tough sustainable bio-based soybean protein adhesive with salt-bridge hydrogen bonds, Int. J. Biol. Macromol. 320 (Pt 3) (2025) 145929, https://doi.org/10.1016/j.ijbiomac.2025.145929.

[6] C.R. Westerman, B.C. McGill, J.J. Wilker, Sustainably sourced components to generate high-strength adhesives, Nature 621 (7978) (2023) 306–311, https://doi.org/10.1038/s41586-023-06335-7.

[7] L. Kong, M. Gao, J. Shi, C. Zhao, C. Chen, Synthetic polypeptide bioadhesive based on cation-pi interaction and secondary structure, ACS Macro Lett. 13 (3) (2024) 361–367, https://doi.org/10.1021/acsmacrolett.4c00075.

[8] H. Chen, Q. Wu, X. Ren, X. Zhu, D. Fan, A fully bio-based adhesive with high bonding strength, low environmental impact, and competitive economic performance, Chem. Eng. J. 494 (2024) 153198, https://doi.org/10.1016/j.cej.2024.153198.

[9] J. Zhang, N. Chen, Z. Zhu, Y. Huang, L. Chen, F. Li, Dual dynamic bonds synergy for reusable bio-based adhesive with superior mechanical robustness, environmental reliability, and mildew resistance, NPG Asia Mater. 17 (1) (2025) 31, https://doi.org/10.1038/s41427-025-00601-y.

[10] T. Deng, D. Gao, X. Song, Z. Zhou, L. Zhou, M. Tao, Z. Jiang, L. Yang, L. Luo, A. Zhou, L. Hu, H. Qin, M. Wu, A natural biological adhesive from snail mucus for wound repair, Nat. Commun. 14 (1) (2023) 396, https://doi.org/10.1038/s41467-023-35907-4.

[11] Y. Ma, X. Zhu, Y. Zhang, X. Li, X. Chang, L. Shi, S. Lv, Y. Zhang, Castor oil-based adhesives: a comprehensive review, Ind. Crop. Prod. 209 (2024), https://doi.org/10.1016/j.indcrop.2023.117924.

[12] X. Zhao, T. Liu, R. Ou, X. Hao, Q. Fan, C. Guo, L. Sun, Z. Liu, Q. Wang, Fully biobased soy protein adhesives with integrated high-strength, waterproof, mildew-resistant, and flame-retardant properties, ACS Sustain. Chem. Eng. 10 (20) (2022) 6675–6686, https://doi.org/10.1021/acssuschemeng.2c00742.
[13] Y. Kan, J. Chang, S. Wei, J. Li, C. Gui, S. Han, Z. Gao, A synergistic strategy for formulating a facile and cost-effective soybean protein-based adhesive via co-crosslinking and inorganic hybridization, Int. J. Biol. Macromol. 283 (Pt 1) (2024) 137569, https://doi.org/10.1016/j.ijbiomac.2024.137569.
[14] C.R. Frihart, C.G. Hunt, Protein structure and wood adhesives, Ind. Crop. Prod. 229 (2025) 121008, https://doi.org/10.1016/j.indcrop.2025.121008.
[15] J. Wei, S. Jia, J. Guan, C. Ma, Z. Shao, Robust and highly sensitive cellulose nanofiber-based humidity actuators, ACS Appl. Mater. Interfaces 13 (45) (2021) 54417–54427, https://doi.org/10.1021/acsami.1c17894.
[16] K. Tachai, A. Deenu, S. Pisutpiched, S. Kamthai, Optimization and addition of bagasse dialdehyde carboxymethyl cellulose (DCMC) as a crosslinking agent for improving the ternary biopolymer blended films: Rice starch, chitosan, and Sericin properties, Int. J. Biol. Macromol. 309 (Pt 3) (2025) 142980, https://doi.org/10.1016/j.ijbiomac.2025.142980.
[17] X. Zhang, T. Liu, Z. Liu, X. Zhu, C. Long, J. Li, Q. Gao, J. Li, P. Song, A bionic strong nanostructured soy protein-based adhesive enabled antistatic and self-extinguishing wood-based composites, Sustain. Mater. Technol. 40 (2024), https://doi.org/10.1016/j.susmat.2024.e00979.
[18] Y. Kan, B. Sun, Y. Bai, Z. Gao, Double-network strategy for a cost-effective soybean meal-based adhesive with required and stable water resistance for structural use, Compos. Pt. B-Eng. 235 (2022), https://doi.org/10.1016/j.compositesb.2022.109744.
[19] X. Liu, J. Li, S. Liu, Z. Zhang, Y. Qing, X. Li, M. Liu, Y. Wu, Mussel and plant cell wall-inspired soy protein adhesives: high strength, flame retardancy, and mildew resistance, Int. J. Biol. Macromol. 320 (Pt 4) (2025) 145875, https://doi.org/10.1016/j.ijbiomac.2025.145875.
[20] Y. Hou, Y. Li, Y. Li, D. Li, T. Guo, X. Deng, H. Zhang, C. Xie, X. Lu, Tuning water-resistant networks in mussel-inspired hydrogels for robust wet tissue and bioelectronic adhesion, ACS Nano 17 (3) (2023) 2745–2760, https://doi.org/10.1021/acsnano.2c11053.
[21] M. Song, H.-K. Park, M. Kim, G.W. Hwang, J. Son, G.R. Kang, J. Lee, C. Pang, Skin-adaptive nanofiber-based adhesive electronics with octopus-like 3D suction cups for enhanced transdermal delivery, npj Flexible Electron. 9 (1) (2025), https://doi.org/10.1038/s41528-025-00433-4.
[22] L. Zhang, Z. Hang, H. Hu, Bio-inspired artificial hair flow sensors: a comprehensive review of design, fabrication, enhancements, and applications, Microsyst. Nanoeng. 11 (1) (2025) 88, https://doi.org/10.1038/s41378-025-00895-6.
[23] S. Hu, S. Wan, X. Zhang, X. Wang, L. Guan, Y. Ge, Y. Li, J. Luo, B. Tang, Structure, production and application of spider silks, Int. J. Biol. Macromol. 309 (Pt 3) (2025) 142939, https://doi.org/10.1016/j.ijbiomac.2025.142939.
[24] Z. Yuan, B. Fang, Q. He, H. Wei, H. Jian, L. Zhang, Molecular dynamics study of the structure and mechanical properties of spider silk proteins, Biomacromolecules 26 (1) (2025) 601–608, https://doi.org/10.1021/acs.biomac.4c01398.
[25] D.H. De Oliveira, V. Gowda, T. Sparrman, L. Gustafsson, R. Sanches Pires, C. Riekel, A. Barth, C. Lendel, M. Hedhammar, Structural conversion of the spidroin C-terminal domain during assembly of spider silk fibers, Nat. Commun. 15 (1) (2024) 4670, https://doi.org/10.1038/s41467-024-49111-5.
[26] Q. Zhang, M. Song, Y. Xu, W. Wang, Z. Wang, L. Zhang, Bio-based polyesters: recent progress and future prospects, Prog. Polym. Sci. 120 (2021), https://doi.org/10.1016/j.progpolymsci.2021.101430.
[27] N.G. Valsange, N. Warlin, S.V. Mankar, N. Rehnberg, B. Zhang, P. Jannasch, Closed-loop chemically recyclable aromatic polyesters based on asymmetric dicarboxylates obtainable from lignocellulose, Green Chem. 27 (20) (2025) 5770–5781, https://doi.org/10.1039/d4gc05572a.
[28] V.J. Patil, S.J. Dhole, V.S. Bhamare, S.S. Bhamare, S.L. Sonawane, V.V. Gite, Bio-based polyester polyurethane acrylate resin: synthesis and application for solventless UV-curable coatings, React. Funct. Polym. 215 (2025), https://doi.org/10.1016/j.reactfunctpolym.2025.106345.
[29] S. Askari, M.M. Hamedi, O. Sevastyanova, Polycarboxylic polyester binders from renewable feedstock for high-performance battery electrodes, J. Electrochem. Energy Convers. Storage 115 (2025), https://doi.org/10.1016/j.est.2025.115838.
[30] T. Iso, T. Ninomiya, S. Kagami, K. Kubota, Y. Sanai, Environmentally-friendly UV-curable coatings utilizing bio-based polyester acrylates, Prog. Org. Coat. 175 (2023), https://doi.org/10.1016/j.porgcoat.2022.107356.
[31] M. Hofmann, M. Machado, A. Shahid, F. Dourado, M. Garrido, J.C. Bordado, J. R. Correia, Pultruded carbon fibre reinforced polymer strips produced with a novel bio-based thermoset polyester for structural strengthening, Compos. Sci. Technol. 234 (2023), https://doi.org/10.1016/j.compscitech.2023.109936.
[32] V.P. Chavan, A.V. Patwardhan, P.R. Gogate, Intensification of epoxidation of soybean oil using sonochemical reactors, Chem. Eng. Process. 54 (2012) 22–28, https://doi.org/10.1016/j.cep.2012.01.006.
[33] R. Teijido, C. Monteserin, M. Blanco, J.L.L. Odriozola, M.I.M. Olabarria, J.L. Vilas-Vilela, S. Lanceros-Méndez, Q. Zhang, L. Ruiz-Rubio, Exploring anti-corrosion properties and rheological behaviour of tannic acid and epoxidized soybean oil-based fully bio-based epoxy thermoset resins, Prog. Org. Coat. 196 (2024), https://doi.org/10.1016/j.porgcoat.2024.108719.
[34] S. Pathan, S. Ahmad, Synergistic effects of linseed oil based waterborne alkyd and 3-isocynatopropyl triethoxysilane: highly transparent, mechanically robust, thermally stable, hydrophobic, anticorrosive coatings, ACS Sustain. Chem. Eng. 4 (6) (2016) 3062–3075, https://doi.org/10.1021/acssuschemeng.6b00024.
[35] Y. Bai, J. Wan, X. Zhang, H. Huo, H. Shi, H. Yang, Y. Yang, X. Ran, G. Du, L. Yang, Bonding wood via an organic-inorganic hybrid adhesive with excellent mechanical and fire resistance properties, Constr. Build. Mater. 457 (2024) 139495, https://doi.org/10.1016/j.conbuildmat.2024.139495.
[36] Y. Jiang, T. Ju, L. Liu, H. Li, Y. Zhang, N. Wang, Z. Lu, M. Wei, D. Min, Y. Xie, J. Li, Y. Wang, S. Xiao, Bonding of wood with high strength and excellent water resistant cellulose colloidal adhesives, Chem. Eng. J. 512 (2025) 162668, https://doi.org/10.1016/j.cej.2025.162668.
[37] K. Jiang, X. Dong, Y. Chen, D. Fan, F. Chu, A room-temperature curing plant protein-based adhesive with high strength and flame retardancy for heat-free adhesion, Adv. Funct. Mater. 34 (39) (2024), https://doi.org/10.1002/adfm.202403490.
[38] Z.U. Nisa Mughal, G. Liman, G. Aylaz, H. Shaikh, S. Memon, M. Andac, Graphene oxide decorated with melamine-imprinted nanobeads for SERS detection of melamine in milk, Spectrochim. Acta A 338 (2025) 126156, https://doi.org/10.1016/j.saa.2025.126156.